

## Conference Proceedings

1<sup>st</sup> International Conference on Atmospheric Dust - DUST2014

# Dust effects on ground-based irradiance measurements

Maria Rita Perrone, Salvatore Romano\*

*Department of Mathematics and Physics, University of Salento, Lecce, 73100, Italy*

---

### Abstract

The short- and long-wave (SW and LW, respectively) radiative effects of dust particles have been evaluated at the surface during the Saharan dust outbreak occurred over South-Eastern Italy from 9 to 13 July, 2012. We have found that a dust loading increase of  $0.13 \text{ g m}^{-2}$  on July 12 at 12:00 UTC was responsible for a SW downward flux ( $F_{\downarrow}$ ) decrease of  $83 \text{ W m}^{-2}$  and a LW- $F_{\downarrow}$  increase of  $55 \text{ W m}^{-2}$  under clear-sky conditions. During the analyzed dust event, the SW Aerosol Forcing Efficiency (AFE) at the surface has ranged from  $-131$  to  $-113 \text{ W m}^{-2}$  per unit AOT at  $440 \text{ nm}$  ( $\text{AOT}_{440}^{-1}$ ) and the LW-AFE has varied from  $31$  to  $15 \text{ W m}^{-2} \text{ AOT}_{440}^{-1}$  for Solar Zenith Angles SZA in the  $52$ - $69^{\circ}$  range.

*Keywords: Dust radiative effects; aerosol forcing efficiency.*

---

### 1. Introduction

The dust role in the Earth's radiation budget is widely recognized and several experiments have been undertaken to investigate the impact of dust aerosols on the Mediterranean radiation budget (e.g., Perrone et al., 2012; Valenzuela et al., 2012). The transport of desert dust to the Mediterranean basin occurs mainly during spring-summer, contributing to one of the highest radiative effects in the world (e.g., Lelieveld et al., 2002). The radiative impact of dust particles is rather complex since they are of large size and exert a significant direct radiative effect on both the short-wave (SW) and the long-wave (LW) radiation. The direct radiative effect of the atmospheric particles is quantified by the Aerosol Radiative Forcing (ARF) and the Aerosol Forcing Efficiency (AFE). The ARF is evaluated as the difference in net fluxes with and without aerosols. The AFE represents the ARF per unit Aerosol Optical Thickness AOT and it is mainly dependent on the particle composition and size (Tafuro et al., 2007). It is worth noting that SW and LW direct radiative effects by dust particles are generally of opposite sign. In particular, the absorption and scattering of dust particles in the LW-domain enhance the greenhouse effect

---

\*Corresponding Author: [salvatore.romano@studenti.unisalento.it](mailto:salvatore.romano@studenti.unisalento.it)

ISSN: 2283-5954 © 2014 The Authors. Published by Digilabs

Selection and peer-review under responsibility of DUST2014 Scientific Committee

DOI:10.14644/dust.2014.013

and as a consequence, the LW-ARF is positive at the surface while the SW-ARF is negative. Hence, it is important to look at the interaction of dust particles with the LW and SW radiation, to properly define how particles alter the energy budget. Several studies have been performed to analyze the radiative effects of dust particles at the surface in the SW spectral range. Perrone et al. (2012) have found by a radiative transfer model that during the Saharan dust outbreak of July 16, 2009 occurred over South-Eastern Italy, the clear-sky and instantaneous SW-AFE varied from  $-100$  to  $-133 \text{ Wm}^{-2}\text{AOT}_{550}^{-1}$  in the  $54\text{-}76^\circ$  Solar Zenith Angle (SZA) range. Valenzuela et al. (2012) have estimated a daily mean value of the surface SW-AFE of  $-74\pm 12$ ,  $-70\pm 14$  and  $-65\pm 16 \text{ Wm}^{-2}\text{AOT}_{440}^{-1}$  during Saharan dust events occurred over South-Eastern Spain from 2005 to 2010 years. Saha et al. (2008) found by a radiative transfer code, that the surface SW-AFE varied within the range  $-78$  to  $-82 \text{ Wm}^{-2}\text{AOT}_{440}^{-1}$ , during the Saharan dust outbreak of June 19, 2006 occurred over the French Mediterranean coastal zone. Note that rather few studies have reported estimates of the dust particle radiative effects on LW radiation. Zhang & Christopher (2003) using observations from devices onboard the Terra satellite have evaluated a clear-sky mean LW-AFE value of  $15 \text{ Wm}^{-2}\text{AOT}_{550}^{-1}$  in September 2000 over the Sahara desert. Then, Hansel et al. (2010) have retrieved by a radiative transfer code, a mean instantaneous LW-AFE value of  $16 \text{ Wm}^{-2}\text{AOT}_{500}^{-1}$  at the surface and in cloud-free conditions over Cape Verde, during the three dust events related to the NAMMA Field Campaign in September 2006. Thus, most of the studies have used models or satellite-based measurements to retrieve the particles radiative effects at the surface during dust outbreaks. Satheesh & Ramanathan (2000) have suggested a method based on radiative flux measurements to evaluate the instantaneous AFE. This method has recently been used by Stone et al. (2011) to estimate the SW- and LW-AFE at the surface during a wildfire event. The method by Satheesh & Ramanathan (2000) is used in this work to evaluate the clear-sky and instantaneous AFE at the surface in the SW and LW range from ground-based irradiance measurements, during the Saharan dust event of July 9-13, 2012 over the Mediterranean region. The instrumentation and methodology descriptions are in Section 2. Main results about the analyzed dust event and the related radiative effects are discussed in Section 3. Final remarks are presented in Section 4.

## 2. Instrumentation and methodology

The measurements analyzed in this study have been performed at the Mathematics and Physics Department of the Salento University in Lecce ( $40.33^\circ\text{N}$ ;  $18.11^\circ\text{E}$ ), South-Eastern Italy. Two Kipp & Zonen pyranometers (CMP 21 model) and pyrgeometers (CGR 3 model) have been used to retrieve upward and downward radiative fluxes in the solar (SW,  $0.31\text{-}2.8 \mu\text{m}$ ) and the terrestrial (LW,  $4.5\text{-}42 \mu\text{m}$ ) spectral range, respectively. Data have been averaged over 2 minutes and stored for subsequent analysis. The total uncertainties associated with the CMP 21 pyranometer and the CGR 3 pyrgeometer measurements are 2 and 3%, respectively. The pyranometers and the pyrgeometers have been located so as to have the horizon free of significant obstacles. Sun/sky photometer measurements performed within the AERONET network (Holben et al., 1998) and co-located in space and time with the irradiance measurements have been used to retrieve the AOT at 440 nm. Only cloud-screened and quality-assured AERONET retrievals (level 2.0) have been considered in this study. The surface SW- and LW-AFE at a fixed SZA have been determined from the slope of the linear fit between the net radiative fluxes and the corresponding AOTs, according to Satheesh & Ramanathan (2000). The error associated with the AFE estimate has been evaluated from the uncertainty in the slope of the least squares linear fit, which depends on

the uncertainty of radiative flux values. The uncertainties of the SZA and AOT values have been neglected. Satellite MODIS images, analytical air-mass back-trajectories, the BSC-DREAM8b model, and aerosol microphysical properties retrieved from AERONET sun/sky photometer measurements have been utilized to identify clear-sky conditions and to determine and evaluate the presence of dust particles at the monitoring site.

### 3. Results and discussion

#### 3.1 Dust event characterization

This work is focused on the Saharan dust outbreak observed over South-Eastern Italy from 9 to 13 July, 2012. Fig. 1a shows the 7-day analytical back-trajectories of July 12, 2012 at 12:00 UTC (<http://aeronet.gsfc.nasa.gov>). Saharan dust particles are advected over South-Eastern Italy from 1000 to 4500 m, in accordance with Fig. 1a. Fig. 1b reports the true-color satellite image by the MODerate resolution Imaging Spectroradiometer – MODIS (<http://modis.gsfc.nasa.gov>; King et al., 1992) at 12:00 UTC of July 10, 2012. The image reveals a large amount of dust particles over South-Eastern Italy.

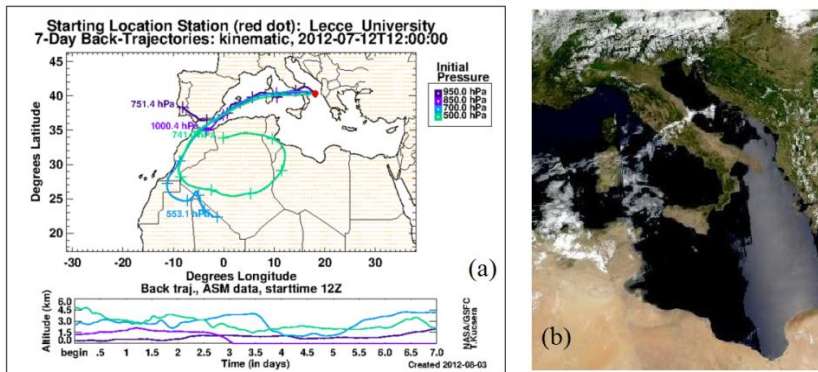


Fig. 1. (a) Pathways of the 7-day back-trajectories at 950, 850, 700, and 500 hPa that reach Lecce on July 12, 2012 at 12:00 UTC (<http://aeronet.gsfc.nasa.gov>). The altitude of each back-trajectory as a function of time is also reported. (b) True-color image of the Central Mediterranean from the MODIS instrument on board the Aqua satellite for July 10, 2012 at 12:00 UTC (<http://modis.gsfc.nasa.gov>).

The BSC-DREAM8b v2.0 model (Basart et al., 2012) has been utilized to quantify the presence of dust particles during the analyzed period. Fig. 2 shows the dust loading (in  $\text{g m}^{-2}$ ) over the Mediterranean estimated by the BSC-DREAM8b forecast model for July (a) 10 and (b) 12, 2012 at 12:00 UTC. In particular, the BSC-DREAM8b model indicates that the dust loading at the monitoring site of this study ( $40.33^\circ\text{N}$ ;  $18.11^\circ\text{E}$ ) was equal to  $0.12 \text{ g m}^{-2}$  and to  $0.15 \text{ g m}^{-2}$  at 12:00 UTC of July 10 and 12, respectively. The Ångström exponent  $\text{Å}(440,870\text{nm})$  retrieved from AERONET sun/sky photometer measurements also confirms the Saharan dust intrusion over South-Eastern Italy. The  $\text{Å}(440,870\text{nm})$  daily mean values were equal to 0.72, 0.74, and 0.64 on July 9, 10 and 12, respectively, and they result significantly lower than the corresponding Å monthly mean value which is equal to 1.29. In fact, Å values smaller than 1 are commonly due to coarse-mode dust and sea-salt particles, while fine-mode particles lead to Å values larger than 1. It is worth noting from the above reported comments that Å reached the smallest value (0.64) when the dust loading estimated by the BSC-DREAM8b reached the largest value ( $0.15 \text{ g m}^{-2}$ ) during the analyzed dust event.

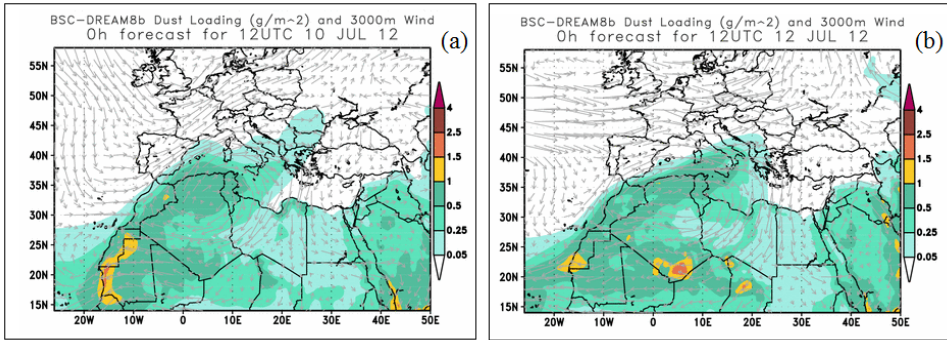


Fig. 2. Dust loading (in  $\text{g m}^{-2}$ ) over the Mediterranean region estimated by the BSC-DREAM8b forecast model for July (a) 10 and (b) 12, 2012 at 12:00 UTC. The wind field pattern is also reported for 3000 m height level.

### 3.2 Radiative flux measurements at the surface

Fig. 3a and 3b show the temporal evolution of the SW and the LW downward flux ( $F\downarrow$ ), respectively, from 8 to 14 July, 2012. Note that the SW- $F\downarrow$  was equal to  $966 \text{ W m}^{-2}$  at 12:00 UTC of July 8 (dust-free day). Then, it decreases up to  $954 \text{ W m}^{-2}$  and  $883 \text{ W m}^{-2}$  at 12:00 UTC of July 9 and 12, respectively, as a consequence of the advection of Sahara dust particles. Conversely, the LW- $F\downarrow$  which was equal to  $403 \text{ W m}^{-2}$  at 12:00 UTC of July 8 increases up to  $458 \text{ W m}^{-2}$  on July 12 (12:00 UTC). The changes of the SW- and LW- $F\downarrow$  peak values with the day are supported by the dust loading estimates from the BSC-DREAM8b model. In fact, the dust loading that was equal to  $0.02 \text{ g m}^{-2}$  at 12:00 UTC of July 8 increases up to  $0.15 \text{ g m}^{-2}$  at 12:00 UTC of July 12.

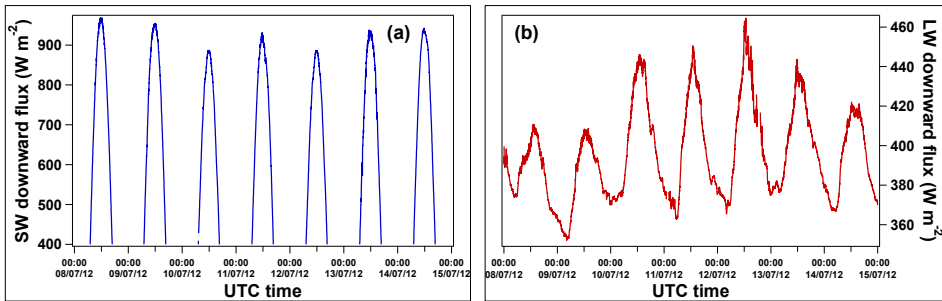


Fig. 3. Temporal evolution of (a) the SW and (b) the LW downward fluxes measured by the CMP21 pyranometer and the CGR3 pyrgeometer, respectively, from 8 to 14 July 2012 at the Lecce monitoring site.

Fig. 4a and 4b show the SW- and the LW- $F\downarrow$  at 12:00 UTC, respectively, versus the corresponding dust loadings retrieved from the BSC-DREAM8b during the analyzed period. The significant effect of the dust loading on the ground-based irradiance measurements is confirmed by the correlation coefficient ( $R$ ) of the best-fitting lines (dotted lines) which is equal to  $-0.76$  (Fig.4a) and  $0.61$  (Fig.4b) in the SW and LW spectral range, respectively.

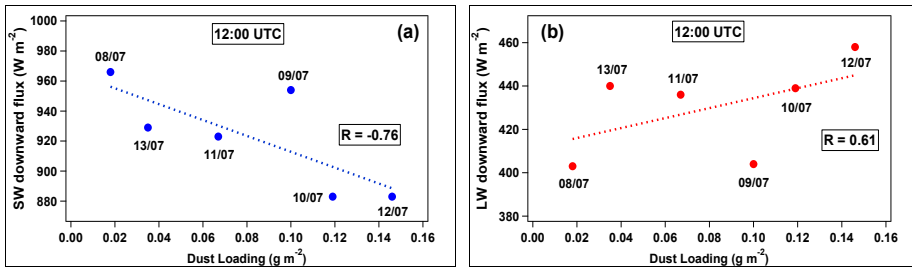


Fig. 4. Scatterplot of the measured downward fluxes in (a) the SW and (b) the LW spectral range versus the dust loading estimated by the BSC-DREAM8b model, from 8 to 13 July 2012 at 12:00 UTC. The dotted line represents the linear fit. The date (dd/mm) and the correlation coefficient R are also reported.

### 3.3 Aerosol forcing efficiency estimates

Fig. 5 shows the dependence of the (a) SW and (b) LW net fluxes on the AERONET AOTs at 440 nm retrieved from measurements performed at  $SAZ = 52^\circ$ , from 9 to 13 July. The slope of the best-fitting line in Fig. 5a, which is equal to  $-131 \text{ Wm}^{-2} \text{ AOT}_{440}^{-1}$ , represents an estimate of the instantaneous SW-AFE at the surface, during the analyzed period. Analogously, the slope of the best-fitting line in Fig. 5b represents the instantaneous LW-AFE at the surface that is equal to  $31 \text{ Wm}^{-2} \text{ AOT}_{440}^{-1}$  during the studied dust event.

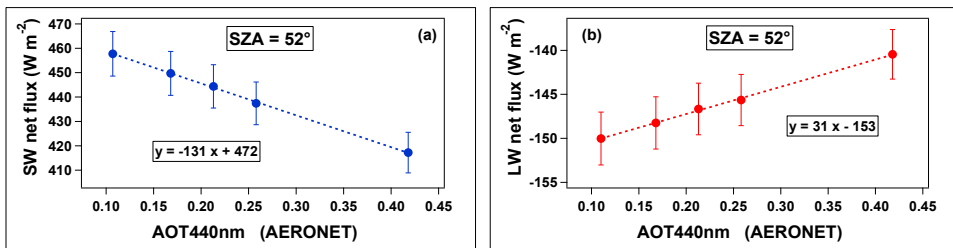


Fig. 5. (a) Linear fit between the measured (a) SW and (b) LW net fluxes and the corresponding aerosol optical thickness AOTs at 440 nm at solar zenith angle  $SAZ = 52^\circ$  from 9 to 13 July, 2012.

Fig. 6 shows the dependence of the (a) SW- and (b) LW-AFE at the surface on the solar zenith angle for the 9-13 July, 2012 time interval. It is worth noting the strong sensitivity of the AFE on the SAZ values and hence on the available sunlight. In particular, Fig. 6a shows that the instantaneous SW-AFE increases from  $-131$  up to  $-113 \text{ Wm}^{-2} \text{ AOT}_{440}^{-1}$  as the SAZ increases from  $52^\circ$  to  $69^\circ$ . Conversely, Fig. 6b reveals a decreasing trend of the

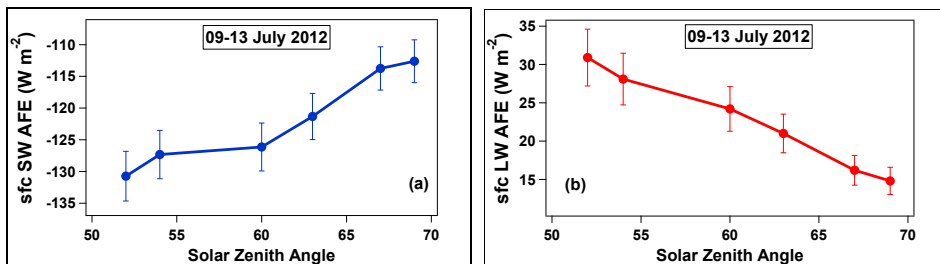


Fig. 6. Scatterplot of the estimated instantaneous (a) SW and (b) LW aerosol forcing efficiencies at the surface versus the related solar zenith angles in  $52-69^\circ$  range, from 9 to 13 July, 2012.

instantaneous LW-AFE as a function of SZA. In particular, it decreases from 31 to 15  $\text{Wm}^{-2}\text{AOT}_{440}^{-1}$  within the 52-69° SZA range.

#### 4. Conclusions

The dust effects on ground-based SW and LW irradiance measurements have been evaluated during the Saharan dust outbreak which has affected South-Eastern Italy from 9 to 13 July, 2012. We have found that the dust loading was equal to  $0.02 \text{ g m}^{-2}$  at 12:00 UTC of 8 July and increased up to  $0.15 \text{ g m}^{-2}$  at 12:00 UTC of July 12. Then, we have observed that the dust loading increase of  $0.13 \text{ g m}^{-2}$  was responsible for the SW-F↓ decrease from 966 to 883  $\text{W m}^{-2}$  and the LW-F↓ increase from 403 to 458  $\text{W m}^{-2}$ . These results reveal the cooling and warming effect by dust particle in SW and LW spectral range, respectively. We have also found that from 9 to 13 July, 2012, the instantaneous SW-AFE increased of 18  $\text{Wm}^{-2}\text{AOT}_{440}^{-1}$  and the instantaneous LW-AFE decreased of 16  $\text{Wm}^{-2}\text{AOT}_{440}^{-1}$  for SZA angles varying within the 52-69° range.

#### 5. Acknowledgements

S. Romano has carried out this work with the support of a PhD fellowship from the Mathematics and Physics Department of the Salento University. This study has been supported by the European Community through the ACTRIS Research Infrastructure Action under the 7th Framework Programme, ACTRIS grant agreement no. 262254. The NASA/Goddard Space Flight Center and the Barcelona Super-Computing Centre are also acknowledged for their contribution of satellite images and DREAM results, respectively.

#### References

- Basart S., Pérez C., Nickovic S., Cuevas E., Baldasano J.M. (2012). Development and evaluation of the BSC-DREAM8b dust regional model over Northern Africa, the Mediterranean and the Middle East. *Tellus Series B* 64, 1-23.
- Hansell R.A., et al. (2010). An assessment of the surface longwave direct radiative effect of airborne Saharan dust during NAMMA field campaign. *Journal of the Atmospheric Sciences* 67, 1048-1065.
- Holben B.N., et al. (1998). AERONET - A federated instrument network and data archive for aerosol characterization. *Remote Sensing of Environment* 66, 1- 16.
- King M.D., Kaufman Y.J., Menzel W.P., Tanré D. (1992). Remote sensing of cloud, aerosol, and water vapor properties from the Moderate Resolution Imaging Spectrometer (MODIS). *Transactions on Geoscience and Remote Sensing* 30, 1-27.
- Lelieveld J., et al. (2002). Global air pollution crossroads over the Mediterranean, *Science* 298, 794- 799.
- Perrone M.R., Tafuro A.M., Kinne S. (2012). Dust layer effects on the atmospheric radiative budget and heating rate profiles. *Atmospheric Environment* 59, 344-354.
- Saha A., Mallet M., Roger J.C., Dubuisson P., Piazzola J., Despiou S. (2008). One year measurements of aerosol optical properties over an urban coastal site: Effect on local direct radiative forcing. *Atmospheric Environment* 90, 195-202.
- Satheesh S.K., Ramanathan V. (2000). Large differences in tropical aerosol forcing at the top of the atmosphere and Earth's surface. *Nature* 405, 60-63.
- Stone R.S., Augustine J.A., Dutton E.G., O'Neill N.T., Saha A. (2011). Empirical determination of the longwave and shortwave radiative forcing efficiencies of wildfire smoke. *Journal of Geophysical Research* 116, D12207.
- Tafuro A.M., Kinne S., De Tomasi F., Perrone M.R. (2007). Annual cycle of aerosol direct radiative effect over southeast Italy and sensitivity studies. *Journal of Geophysical Research* 112, D20202.
- Valenzuela A., Olmo F.J., Lyamani H., Anton M., Quirantes A., Alados-Arboledas L. (2012). Aerosol radiative forcing during African desert dust events (2005–2010) over Southeastern Spain. *Atmospheric Chemistry and Physics* 12, 10331-10351.
- Zhang J., Christopher S.A. (2003). Longwave radiative forcing of Saharan dust aerosols estimated from MODIS, MISR and CERES observations on Terra. *Geophysical Research Letters* 30, 2188.